Center-to-limb line width measurements
of solar chromospheric, transition region and coronal lines

R. Erdélyi[1,2], J.G. Doyle[2], M.E. Perez[2], and K. Wilhelm[3]

[1] School of Mathematical and Computational Sciences, University of St. Andrews, North Haugh, St. Andrews. Fife, KY16 9SS, UK
   (robertus@dcs.st-and.ac.uk)
[2] Armagh Observatory, College Hill, Armagh BT61 9DG, Northern Ireland (robert@star.arm.ac.uk, jgd@star.arm.ac.uk, epp@star.arm.ac.uk)
[3] Max-Planck-Institut für Aeronomie, D-37191 Katlenburg-Lindau, Germany, (wilhelm@Linmpi.mpg.de)

Abstract. Line widths derived from observational data obtained by SUMER onboard SOHO in August 1996 at disk center and at the limb are used to confront those derived via assuming Alfvén and/or magneto-acoustic wave heating. The observational data clearly shows a center-to-limb variation in the upper chromospheric and transition region lines, with only a marginal difference in the coronal lines in the sense of additional broadening further from disk center. Numerical estimations based on *linear* MHD, favour the existence of Alfvén wave heating over magneto-acoustic heating, although further calculations are required. For example, non-linear effects could change the wave characteristics which in turn can have a major effect on the overall line broadening.

Key words: line: profiles – waves – Sun: chromospheres – Sun: corona – Sun: transition region

1. Introduction

In the solar atmosphere the initial decrease of temperature down to 4300 K at the temperature minimum is followed by an enormous increase with increasing distance from the photosphere. This increase is gradual in the chromosphere but very steep in the lower part of the solar corona where the temperature reaches up to $2,000,000$ K. This temperature increase is one of the most challenging observational facts for theorists in plasma-astrophysics. The high temperature of the solar corona is only possible if there is a non-thermal heating mechanism that is continuously working. Biermann (1946) and Schwarzschild (1948) suggested that the corona may be heated by sound waves. Until the mid 70's this acoustic wave heating model was accepted by most theorists. However, this model was largely abandoned when it became clear from UV observations, that the energy flux of the acoustic waves is too small in the upper part of the solar atmosphere to account for the observed radiative losses.

The X-ray observations from Skylab showed that more than 90% of the X-ray flux originates from closed loops with the

heating being directly linked to the solar magnetic field. The source of this heating has to be the convection zone which is a huge reservoir of kinetic energy. The real problem is to explain how a fraction of this kinetic energy is transported to the coronal layers and how it is dissipated and converted into heat there.

There are three broad classical branches of theories for plasma heating that have been considered during the last two decades: Alfvén wave heating, resistive dissipation of direct electric currents and selective decay of a turbulent cascade of magnetic fields. The literature on these theories has undergone a recent expansion (see, e.g., Browning, 1991; Cargill, 1993; Forbes, 1991; Gomez, 1990; Heyvaerts, 1990; Hollweg, 1991; Narain & Ulmschneider, 1990,1996; Melrose, 1990; Priest, 1990 and Zirker, 1993).

In this paper we consider observations obtained by the SUMER (Wilhelm et al. 1995) instrument on the Solar and Heliospheric Observatory spacecraft (SOHO) to look for signatures of wave heating. Practically there are two possibilities for detecting wave activity in the solar atmosphere: (i) the first is via measuring directly the individual intensity oscillations if these oscillations can be resolved spatially (e.g., Doyle et al. 1997, 1998); or (ii) measure the averaged effect of oscillations in the broadening of optically thin emission lines. The latter being the subject of the present paper.

There have been numerous measurements of line widths, e.g., Boland et al. (1975), Moe & Nicholas (1977), Cheng et al. (1979), and Mariska et al. (1978, 1979). All the different estimations involving wave heating have assumed that the observed non-thermal broadening is isotropic in nature, i.e., it has the same magnitude at disk center and at the limb. Previous results have tended to support this assumption (Mariska et al., 1978), although Roussel-Dupré et al. (1979) did suggest a center-to-limb variation. Here we look again at this question analysing observational data taken at different locations on the solar disk and comparing these to calculated widths assuming different types of wave heating.

Note that although MHD (Alfvén) waves are good candidates to explain the center-to-limb line broadening, there can also be other physical processes responsible for this, e.g., turbulent line broadening produced by nanoflares (e.g., Cargill 1996),

---

explosive events (e.g., Innes et al. 1997, Erdélyi et al. 1997, 1998, Sarro et al. 1997).

The high spectral and spatial resolution capabilities of SUMER can enable a search for Alfvén and/or magneto-acoustic waves in the solar atmosphere via an observational sequence as suggested by McClements et al. (1991). The original idea was to select an active region loop at disk center, measuring the widths in different high temperature lines as the loop moved towards the limb. If Alfvén waves are dominant in the coronal loop than there should be a broadening of the line widths from disk center to limb. However, if the magneto-acoustic waves have the dominant contribution, the width of the lines should decrease. Before attempting this type of observation we choose to observe an average quiet Sun region at disk center and at the limb, measuring the widths of lines formed at chromospheric and coronal temperatures.

2. Observations

2.1. The data

SUMER is a normal incidence spectrograph operating over the wavelength range 400 Å to 1610 Å. The off-axis parabola mirror is movable in two dimensions around the focal point allowing pointing of the instrument independent of the spacecraft pointing. Four slits are available: 4×300, 1×300, 1×120, and 0.3×120 arc sec^2. For the data obtained here we used the 1×300 arc sec^2 slit. Both 1st and 2nd orders are superimposed on the detector, with the dispersion in wavelength varying from 45 mÅ/pixel (1st order) to 22.5 mÅ/pixel (2nd order) at 800 Å to 41.8 mÅ/pixel and 20.9 mÅ/pixel at 1600 Å. The detector (see Siegmund et al. 1994) has 1024 spectral pixels and 360 spatial pixels. The central area is coated with KBr which increases the quantum efficiency by an order of magnitude in the range 900 Å to 1500 Å.

The observations reported here were obtained on 3rd and 4th Aug 1996 using exposure times of 300 s with detector A. After each exposure, the slit was moved by 1.1 arc sec, accumulating an image covering an area of 30×300 arc sec^2. At each of the three solar locations (disk center, 800 arc sec from the center and the limb), data was obtained for three spectral settings, 1041 Å, 1245 Å, and 1352 Å each covering 40 Å. The objective of the observing programme was to obtain a good mean quiet Sun spectrum. In deriving the mean spectrum, the maximum number of individual scans was thirty, however some of these were unusable. Below we give more details:

– **DISK CENTER** For the files with reference wavelength = 1041 Å we took the mean of 27 spectral scans with XCEN/YCEN between -15.75/0.0 and 14.62/0.0 (i.e., in arc sec from disk center where positive X is West and positive Y in North). For the files with reference wavelength = 1245 Å we took the mean of 19 spectral scans with XCEN/YCEN between 13.87/0.0 and 37.62/0.0, and finally, for the files with reference wavelength = 1352Å we took the mean of 17 spectral scans with XCEN/YCEN between 47.75/0.0 and 65.25/0.0.
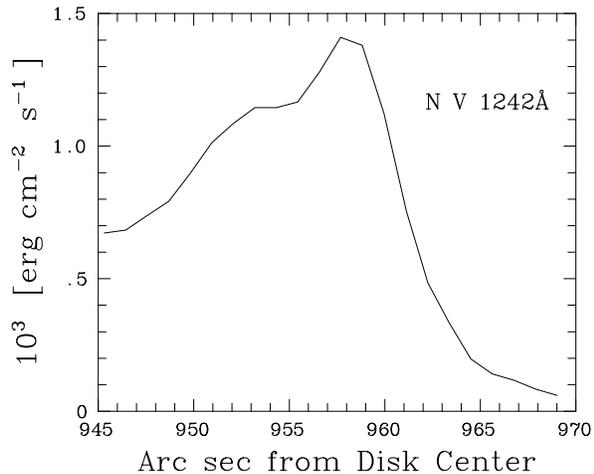

Fig. 1. The N V 1424 Å line flux as a function of position in arc sec from disk center for the limb observations

– **800 arc sec from disk center** For the files with reference wavelength = 1041 Å we took the mean of 30 spectral scans with XCEN/YCEN between 785.37/0.0 and 815.81/0.0.
– **LIMB-A** For the files with reference wavelength = 1041 Å we took the mean of 15 spectral scans with XCEN/YCEN between 936.25/0.0 and 956.56/0.0. For the files with reference wavelength = 1245 Å we took the mean of 12 spectral scans with XCEN/YCEN between 946.44/0.0 and 956.56/0.0, and for the files with reference wavelength = 1352 Å the mean of 12 spectral scans with XCEN/YCEN between 945.69/0.0 and 955.81/0.0.
– **LIMB-B** For files with reference wavelength = 1041 Å we took the mean of 6 spectral scans with XCEN/YCEN between 963.37/0.0 and 966.75/0.0. For files with reference wavelength = 1245 Å we took the mean of 8 spectral scans with XCEN/YCEN between 963.37/0.0 and 970.12/0.0, and for the files with reference wavelength = 1352 Å the mean of 18 spectral scans with XCEN/YCEN between 959.19/0.0 and 976.12/0.0.

Thus the LIMB-A data refers to observations taken up to and including the limb, whereas the LIMB-B data refers to data taken several arc sec off-limb. In Fig. 1 we show the N V 1242 Å line flux as a function of position in arc sec from disk center for the limb observations derived by integrating over the entire slit for each scan position.

Each spectral scan was checked for the presence of explosive events as these can cause localised line broadening. Considering that the integration time was 300 s per spectrum, detection of such events is difficult. Although some spatially small brightenings ($\sim 5-6$ arc sec) are present in one or two spectra, these do not affect the average, as for example in the disk center spectrum we average over an area of 300×27 arc sec^2 for data involving O VI and 300×19 arc sec^2 for data involving N V.

Table 1. A summary of the measured $FWHM$ in mÅ, plus the derived Doppler width corrected for instrumental broadening for lines formed in the solar chromosphere to the corona

Line (Å)	Disk-Center		800 arc sec from center		Limb-A		Limb-B	
	FWHM	Doppler	FWHM	Doppler	FWHM	Doppler	FWHM	Doppler
C I 1252.2	121	53			134	64	138	67
S I 1050.3	118	51	117	50	129	60	160	83
S II 1253.7	144	71			201	110	222	124
Fe II 1368.1	109	43			133	63	179	96
S III 683.5 (2nd)	217	121			235	132	247	140
O I 1041.7	125	57	135		150	75	144	71
Cl I 1351.7	113	47			127	58	138	67
C II 1036.3	163	85	193	105	241	127	214	119
S IV 1062.7	194	106	203	112	194	106	216	120
N III 684.9 (2nd)	233	131			276	158	283	163
N V 1242.8	224	125			255	145	285	164
O VI 1037.6	225	126	239	135	254	144	275	158
Na IX 681.6 (2nd)	280	161			285	164	297	171
O V 629.5 (2nd)	227	127			277	159	309	179
Mg X 624.9 (2nd)	268	153			283	163	288	166
Fe XII 1242.0	227	127			215	119	227	127

2.2. Data reduction

For the SUMER instrument, the process of data reduction involves three main steps; destretching, radiometric calibration and slit effects correction (these datasets were automatically flat-field corrected onboard the satellite). Destretching of the SUMER datasets is necessary, particularly for the data towards the end of the slit due to various wavelength and spatial distortions in the detector. After ruling out unusable files, due to errors in the headers, bad data, etc., all the images obtained at different scan positions (for a determined wavelength range and solar position) were averaged in order to improve the signal to noise. Due to problems towards the end of the slit, only the spatial pixels [26, 310] were considered in deriving the averaged spectrum. Conversion of the SUMER count rates into physical units was via the radiometric calibration of Wilhelm et al. (1997). The final step in the process was the correction to the measured line widths for the effects of the slit used. The magnitude of this correction is small, although it can result in a correction of ~ 2 km s^{-1} in the derived non-thermal velocities (see later). The above corrections were done using various IDL routines from within the SUMER software tree (e.g., $DESTRETCHN.PRO$, $RADIOMETRY.PRO$, $CON\_WIDTH\_2.PRO$, and finally, $CON\_WIDTH\_FUNCT\_2.PRO$). Spectral line fitting was via $CFIT.PRO$ from the CDS software tree.

3. Results

Gaussian profiles were fitted to each spectral line (for some ions we had two or more lines at different wavelengths although in many instances these additional lines were weak). As found previously all of the measured line widths are in excess of their thermal width for all solar locations. This excess width may be associated with velocity fields. When the scale of these motions is small compared with the instrumental resolution, they are often accounted for by adding a component (ξ) to the Doppler width

$$\Delta\lambda_D^2 = \frac{\lambda^2}{c^2}\left(\frac{2kT}{M_i} + \xi^2\right), e \tag{1}$$

Table 2. The derived non-thermal velocities (ξ) for the different regions based on the measured line width given in Table 1. The estimated error in ξ is $\pm$1-2 km s^{-1}.

Line (Å)	log T	Disk Center	800 arc sec	Limb A	Limb B
C I 1252.2	4.10	12		14	15
S I 1050.3	4.10	12	12	14	19
Cl I 1351.7	4.10	10		13	14
Fe II 1368.1	4.10	9		14	21
O I 1041.7	4.15	16	18	21	20
S II 1253.7	4.30	16		26	29
C II 1036.3	4.50	24	30	39	34
S III 683.5	4.70	26		29	30
N III 684.9	4.90	27		33	34
S IV 1062.7	5.00	29	30	29	33
N V 1242.8	5.30	26		32	36
O V 629.5	5.40	26		34	36
O VI 1037.6	5.50	32	34	38	42
Na IX 681.6	5.90	26		27	29
Mg X 624.9	6.00	26		29	30
Fe XII 1242.0	6.20	22		19	22

where ξ is the most probable non-thermal velocity, and M_i the ion mass. This, of course, assumes that the non-thermal velocities also have a Gaussian distribution. Furthermore, additional broadening due to the instrument must first be removed. The temperatures used are the ionisation equilibrium temperatures of Arnaud & Rothenflug (1985) and Arnaud & Raymond (1992).

A summary of the derived line widths for the strongest lines are given in Table 1. The difference in the derived non-thermal velocities at disk center compared to those just inside the limb and those outside the limb are given in Fig. 2. Here we see a clear difference in two different temperature regimes, 20,000 K and 250,000 K. Both of these temperature regimes indicate excess line broadening at the limb compared to disk center. It should also be noted that the data taken at 800 arc sec from disk center also shows additional broadening, although the number of lines observed is smaller. In deriving ξ, an instrumental width of 77 mÅ was used. Several of the low temperature lines measured on-disk (e.g., Fe II, Cl I) have measured FWHM close to 110 mÅ which translates to a FWHM of 73 mÅ (or a Doppler width of 44 mÅ) when the instrumental correction is applied.

The range of non-thermal velocities in Table 1 are in very good agreement with values obtained previously by other authors, e.g., Hassler et al. (1990) obtain 26 km s^{-1} for Mg X at disk center, Cheng et al. (1979) obtained for the solar limb values ranging from 10 to 25 km s^{-1} for Fe XII while Doyle et al. (1997) obtained $12 - 30$ km s^{-1}. For O VI at disk center, Warren et al. (1997) obtained 33 km s^{-1}, while Doschek et al. (1981) obtained 27 km s^{-1} for N V.

4. Discussion

The observed increase in the Limb B (> 960 arc sec) line widths over those at Limb A (< 956 arc sec) in the mid-transition re-
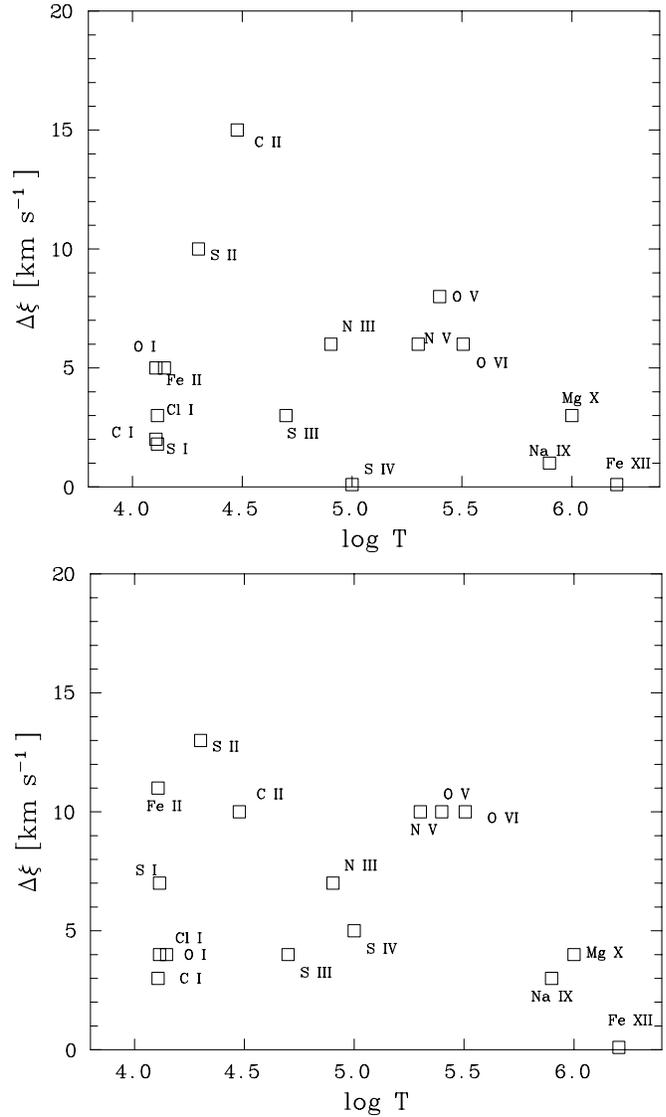

Fig. 2. The excess non-thermal velocities in lines from the chromosphere to the corona for Limb A (top panel, i.e., just inside the limb) and Limb B (bottom panel, just outside the limb) compared to that at disk center. The estimated error in the derived ξ is $\pm$1-2 km s^{-1}

gion are consistent with previous results (e.g., Shine et al. 1976, Mariska et al. 1978). Published results of on-disk measurements of center-to-limb variations is however more limited. For example, Feldman et al. (1976) concluded that the line widths of several optically thin lines were similar at disk center and the limb. Exceptions to this were the strong resonance lines of C IV and Si IV, which were explained in terms of opacity effects. The data presented in Fig. 2a suggests a center-to-limb variation which we believe cannot be explained by optical depth effects.

The maximum difference seems to occur at two different temperature regimes; the first at 20,000 K and the second at 250,000 K, with little or no difference at lower chromospheric temperatures or coronal temperatures. The lines with the highest probability of being affected by opacity are the lower temperature lines, notably C II. In Table 3 we tabulate the line ratios

Table 3. The line ratio for the various doublets observed in this programme

Line Ratio	Disk Center	800 arc sec	Limb A	Limb B
S II 1253.7/1250.5	1.96		1.75	1.91
C II 1036.3/1037.0	0.92	0.91	0.95	0.78
N V 1238.8/1242.8	1.86		1.87	1.84
O VI 1031.9/1037.6	2.07	2.10	1.67	1.78

of the various doublets. As can be seen, the C II lines are optically thick everywhere, while the remaining lines are effected by opacity mostly for the Limb A data. Thus the C II data-point plotted in Fig. 2a (i.e., Limb-A) could be affected by opacity although the line ratio from Table 3 indicates a similar effect at disk center and the limb, thus whether the difference (limb minus disk center) is seriously affected is unclear. For the Limb-B data, (Fig. 2b), the data-points for C II, S II and Fe II are all in very good agreement, furthermore Table 3 indicates only a small line opacity effect for S II. Our data at 250,000 K include the weaker component of the strong resonance lines of N V and O VI, the stronger component showing a slightly larger line width suggesting opacity effects. Also included here is the resonance line of O V 630 Å. Thus we do not ascribe all of the excess (limb minus disk center) broadening in Figs. 2a,b to opacity. The important message to note from these figures is the clear excess limb minus disk center broadening.

Roussel-Dupré et al. (1979) in a detailed analysis of Si IV 1393, showed that this line undergoes a marked broadening from disk center to the limb. Their Fig. 1 indicates additional broadening at $\mu \sim 0.5$ compared to $\mu \sim 1.0$ (disk center). At disk center their Si IV line has a $1/e$ half-width of 0.09 Å compared to 0.105 Å at $\mu \sim 0.5$, indicating excess broadening equivalent to $\sim$ 3km s^{-1}. This suggested that horizontal velocities were somewhat greater than the radial velocities, similar to the results reported here. As in the Feldman et al. results, some of this could be explained by optical depth effects. Mariska (1992) suggests that the difference in line width can be accounted for with a small increase in opacity depth.

The solar atmosphere is a highly non-uniform plasma embedded in a magnetic field which is a natural media for MHD waves. MHD waves might play an important role in explaining the observed high temperatures (i.e., $\sim$ 2 10^6 K) in the solar corona. These waves can be generated either by the granular motions (e.g., foot-point motions) or excited locally by magnetic reconnection, with part of their kinetic energy being transformed into heating the magnetic loops. In this paper we do not study how MHD waves are excited, we suppose *a priori* they are present in the solar atmosphere. Furthermore, we suppose that such waves can propagate along the magnetic field lines and carry energy to the higher parts of the atmosphere. We also do not discuss how this energy is dissipated and converted into heat.

We are more concerned with a method of testing their existence via calculating the contribution of wave broadening to the overall line widths. This wave broadening is strongly influenced by the orientation of the magnetic field with respect to the line of sight and the polarisation of the waves.

Below we derive line widths calculated assuming (i) Alfvén wave heating and (ii) magneto-acoustic wave heating for comparison with the observational data. In the analysis which follows we assume an isothermal and uniform plasma.

4.1. An estimate of line widths as a result of Alfvén waves

Observations show that the aspect ratio ϵ of coronal loops are much larger than unity, i.e., coronal loops can be approximated by straight cylindrical magnetic flux tubes. The very high electrical conductivity of coronal plasma enables us to describe the induced electrical field due to wave motion by the ideal Ohm's law,

$$\mathbf{E} + \frac{1}{c}\mathbf{v} \times \mathbf{B} = 0. \tag{2}$$

By supposing that there is no background equilibrium motion in the plasma, a travelling Alfvén wave along a magnetic field line **B** results in a velocity perturbation $\delta\mathbf{v}$ of a perfectly conducting plasma,

$$\delta\mathbf{v} = \frac{\delta\mathbf{E} \times \mathbf{B}}{B^2}c, \tag{3}$$

where c is the speed of light, and $\delta\mathbf{E}$ is the induced electrical field caused by the Alfvén wave.

The energy flux associated with an Alfvén wave propagating along the magnetic field lines is

$$\Phi = \left(\frac{\langle\delta\mathbf{B}^2\rangle}{8\pi} + \frac{\langle\delta\mathbf{E}^2\rangle}{8\pi} \right) v_A, \tag{4}$$

where $\delta\mathbf{B}$ is the perturbation of the magnetic field caused by the Alfvén wave, and v_A denotes the Alfvén speed. In solar applications $c \gg v_A$, and by using

$$\langle\delta\mathbf{B}^2\rangle = \frac{c^2}{v_A^2}\langle\delta\mathbf{E}^2\rangle \gg \langle\delta\mathbf{E}^2\rangle, \tag{5}$$

so that,

$$\Phi \sim \frac{c^2}{v_A^2}\frac{\langle\delta\mathbf{E}^2\rangle}{8\pi}, \tag{6}$$

or

$$\Phi = n_e m_p \langle v_\parallel^2 \rangle v_A, \tag{7}$$

where n_e is the plasma electron density, and m_p denotes the proton mass. Here we assume random polarisation, in which case the mean-square velocity component towards an observer is given by

$$\langle v_\parallel^2 \rangle = \frac{1}{2}\langle v^2 \rangle. \tag{8}$$

Table 4. The calculated excess Doppler line broadening in km s^{-1} at the two limb positions A & B compared to disk center for the ions given in Table 1 for cool loops assuming (i) Alfvén waves and (ii) acoustic waves. Here we used $\Phi = 4 \times 10^6$ erg cm^{-2} s^{-1}, $B = 25$ G, and $n_e = 5.6 \times 10^{10}$ cm^{-3} (see text).

Line (Å)	Alfvén waves	acoustic waves	observ.	
			A	B
C I 1252.2	16	−58	3	3
S I 1050.3	17	−60	3	9
Cl I 1351.7	17	−60	2	4
O I 1041.7	16	−59	5	4
S II 1253.7	17	−52	9	13
C II 1036.3	15	−45	15	11
Fe II 1368.1	17	−53	4	12

Table 5. The calculated excess Doppler line broadening in km s^{-1} at the two limb positions A & B compared to disk center for the ions given in Table 1 for hot loops assuming (i) Alfvén waves and (ii) acoustic waves. Here we used $\Phi = 4 \times 10^6$ erg cm^{-2} s^{-1}, $B = 125$ G, and $n_e = 2 \times 10^9$ cm^{-3} (see text).

Line (Å)	Alfvén waves	acoustic waves	observ.	
			A	B
S III 683.5	15	−214	2	4
N III 684.9	12	−186	6	7
S IV 1062.7	14	−177	-	4
N V 1242.8	10	−141	5	9
O V 629.5	9	−131	8	12
O VI 1037.6	9	−121	5	9
Na IX 681.6	7	−89	1	2
Mg X 624.9	6	−77	2	3
Fe XII 1242.0	8	−73	-	-

Let us estimate the line broadening due to a propagating Alfvén wave. For a thermally broadened line produced by an ion of mass M_i, the Doppler temperature is given by

$$kT_D = kT + M_i \langle v_{\parallel}^2 \rangle. \tag{9}$$

Using the above equations, this implies, that line broadening caused by an Alfvén wave travelling along the magnetic field lines (which is perpendicular to the line of sight) can be estimated as

$$\frac{\Delta \lambda_D}{\lambda} = \frac{1}{c} \left(\frac{2kT}{M_i} + \frac{4\pi^{1/2}\Phi}{(n_e m_p)^{1/2} B} \right)^{1/2}, \tag{10}$$

where $\Delta \lambda_D$ is the Doppler width given in Table 1.
When, however, the magnetic field is directed towards the observer, (i.e., the oscillations caused by Alfvén waves are perpendicular to the line of sight), the line width is given by

$$\frac{\Delta \lambda_D}{\lambda} = \frac{1}{c} \left(\frac{2kT}{M_i} \right)^{1/2}. \tag{11}$$

The second set of parameters within the brackets in Eq. (10) does not contain a temperature dependent term and is equated with the measured non-thermal line broadening parameter ξ (see Eq. 1). For the values of n_e, B, and Φ given in Tables 4 & 5 for the hot and cool loops, $\xi = 19$ km s^{-1}. An alternative way of comparing with the observational results is given in Tables 4 & 5. Here, the estimated excess Doppler line broadening at the limb compared to disk center due to the passage of purely Alfvén waves are compared with those derived from the data given in Table 1.

4.2. An estimate of the line width as a result of magneto-acoustic waves

In the previous section we have assumed a linear dispersion relation for the Alfvén waves, i.e., the Alfvén waves had a group

velocity v_A. Generalising this to any wave mode we can replace the group velocity in Eq. (7) by the group velocity of the wave. Let us suppose that there are magneto-acoustic waves travelling *along* the magnetic field lines. In a low-beta plasma like the solar corona these waves show the characteristics of sound waves, i.e., the group velocity can be expressed by

$$v_g = \left(\frac{2\gamma kT}{m_p} \right)^{1/2}, \tag{12}$$

where γ is the ratio of specific heats. These special magneto-acoustic waves have oscillations only along the magnetic field lines, the perturbations perpendicular to the field lines are identically zero. Following the method given in the previous subsection, when the magnetic field lines coincide with the line of sight, one can observe line broadening caused by the magneto-acoustic waves passing along the field lines, e.g.,

$$\frac{\Delta \lambda_D}{\lambda} = \frac{1}{c} \left(\frac{2kT}{M_i} + \frac{2\Phi}{n_e (6m_p kT)^{1/2}} \right)^{1/2}. \tag{13}$$

However when the magnetic field lines are perpendicular to the line of sight, the magneto-acoustic waves travelling along the magnetic field lines do not cause any additional line broadening, i.e., the line width is described by Eq. (11). This shows that pure Alfvén waves and these type of magneto-acoustic waves show opposite behaviour as regards the line width and the direction of the magnetic field. The estimated line widths due to the passage of these magneto-acoustic waves are shown in Tables 4 & 5.

5. Conclusions

The observational data presented here (see Fig. 2 or Table 2) suggests a center-to-limb variation, namely *broadening*, for the

upper chromospheric and transition region lines. Calculated excess line widths assuming magneto-acoustic waves display the opposite effect, while those calculated assuming Alfvén waves have the correct order of magnitude (see last columns in Tables 4 & 5). The values used for the electron density, energy flux, etc. were average values taken from, e.g., McClements et al. (1991), Mariska (1992), and Bray et al. (1991). Changes of less than a factor of two in these values could reduce the difference between theory and observation.

However, we do not want to 'arrange' these input constants to 'fit' the observed line broadening. The uncertainty in the energy flux of the different MHD waves is large. The same is true for the density and topology of the magnetic field (effect of curvature, etc.). Besides these arguments we are more concerned about the errors introduced by the linear approximation of the calculations. Erdélyi & Goossens (1995), Ruderman et al. (1997) and Ballai et al. (1998) showed that nonlinear effects are very important when studying wave propagation and the related heating of the solar corona. The observations presented here (and elsewhere) clearly show excess broadening even at disk center while the linear Alfvén assumption assumes a thermally broaden line at disk center only. Consideration of such effects are, however, outside of the scope of the present study. Nonlinear relations can change the characteristics of the travelling waves which, in turn, could have an important effect on the line broadening.

References

Arnaud, M. & Raymond, J.C. 1992, ApJ, 398, 394

Arnaud, M. & Rothenflug, R. 1985, A&AS, 60, 425

Ballai, I., Ruderman, M.S. & Erdélyi, R. 1998, Phys. Plasmas, 5, 252

Biermann, L. 1946, Naturwissenschaften, 33, 118

Boland, B.C., Dyer, E.P., Firt, J.G., Gabriel, A.H., Jones, B.B., Jordan, C., McWhirter, R.W.P., Monk, P. & Turner, R.F. 1975, MNRAS, 171, 697

Bray, R.J., Cram, L.E., Durrant, C.J. & Loughhead, R.E. *Plasma Loops in the Solar Corona*, Cambridge Univ. Press, 1991

Browning, P.K. 1991, Plasma Phys and Contr. Fus., 33, 539

Cargill, P.J. in J.L. Birch & J.H. Waite, Jr. (eds) *Solar System Plasma Physics: Resolution of Processes in Space and Time*, Proc. of Yosemite Conf., 1993

Cargill, P.J. 1996, Sol. Phys., 167, 267

Cheng, C.C., Doschek, G.A. & Feldman, U. 1979, ApJ, 227, 1037

Doschek, G.A., Mariska, J.T. & Feldman, U. 1981, MNRAS, 195, 107

Doyle, J.G., van den Oord, G.H.J. & O'Shea, E. 1997, A&A, 327, 365

Doyle, J.G., van den Oord, G.H.J., O'Shea, E. & Banerjee, D. 1998, Sol. Phys. (in press)

Erdélyi, R. & Goossens, M. 1995, A&A, 294, 575

Erdélyi, R., Perez, E.P. & Doyle, J.G. in *The Corona and Solar Wind Near Minimum Activity*, ESA-SP 404, 353, 1997

Erdélyi, R., Sarro, L.M. & Doyle, J.G. in *Solar Jets and Coronal Plums*, ESA-SP 421, 207 1998

Feldman, U., Doschek, G.A. & Patterson, N.P. 1976, ApJ, 209, 270

Forbes, T.G. 1991, Geophys. Astrophys. Fluid Dyn., 62, 13

Gomez, D.O. 1990, Fund. Cosmic Phys., 14, 131

Hassler, D.M., Rottman, G.J., Shoub, E.C. & Holzer, T.E. 1990, ApJ, 348, L77

Heyvaerts, J. in R.E. Priest & V. Krishnan (eds.) *Basic Plasma Processes on the Sun*, IAU Symp. 142, 207, 1990

Hollweg, J.V. in P. Ulmschneider, R.E. Priest and R. Rosner (eds.) *Mechanisms of Chromospheric and Coronal Heating* Springer-Verlag, Berlin, p. 423, 1991

Innes, D.E., Inhester, B., Axford, W.I. & Wilhelm, K. 1997, Nature, 386, 811

Mariska, J.T., Feldman, U. & Doscheck, G.A. 1978, ApJ, 226, 698

Mariska, J.T., Feldman, U. & Doscheck, G.A. 1979, A&A, 73, 361

Mariska, J.T. *The Solar Transition Region*, Cambridge Astrophysics Series, 1992

McClements, K.G., Harrison, R.A. & Alexander, D. 1991, Sol. Phys., 131, 41

Melrose, D.B. 1990, Australian J. Phys, 43, 703

Moe, O.K. & Nicholas, K.R. 1977, ApJ, 211, 579

Narain, U. & Ulmschneider, P. 1990, Sp. Sci. Rev., 54, 377

Narain, U. & Ulmschneider, P. 1996, Sp. Sci. Rev., 75, 453

Priest, E.R. 1990, Mem. Soc. Astron. Ital., 61, 383

Ruderman, M.S., Hollweg, J.V. & Goossens, M. 1997, Phys. Plasmas, 4, 75

Roussel-Dupré, R., Francis, M.H. & Billings, D.E. 1979, MNRAS, 187, 9

Sarro, L.M., de Sterck, H., Erdélyi, R., Montesinos, B. & Doyle, J.G. in *The Corona and Solar Wind Near Minimum Activity*, ESA-SP 404, 657, 1997

Schwarzschild, M. 1948, ApJ, 107, 1

Shine, R.A., Roussel-Dupré, R., Bruner, E.C., Chipman, E.G., Lites, B.W., Rottman, G.J., Athay, R.G. & White, O.R. 1976, ApJ, 210, L107

Siegmund, O.H.W., Gummin, M.A., Stock, J.M., Marsh, D., Raffanti, T., Sasseen, T., Tom, J., Welsh, B., Gaines, G.A., Jelinsky, P. & Hull, J. Proc SPIE 2280, 89, 1994

Warren, H.P., Mariska, J.T., Wilhelm, K. & Lemaire, P. 1997, ApJ, 484, L91,

Wilhelm, K., Curdt, W., Marsch, E., Schühle, U., Lemaire, P., Gabriel, A., Vial, J.-C., Grewing, M., Huber, M.C.E., Jordan, S.D., Poland, A.I., Thomas, R.J., Kühne, M., Timothy, J.G., Hassler, D.M. & Siegmund, O.H.W. 1995, Sol. Phys., 162, 189

Wilhelm, K., Lemaire, P., Curdt, W., Schühle, U., Marsch, E., Poland, A.I., Jordan, S.D., Thomas, R.J., Hassler, D.M., Huber, M.C.E., Vial, J.-C., Kühne, M., Siegmund, O.H.W., Gabriel, A., Timothy, J.G., Grewing, M., Feldman, U., Hollandt, J. & Brekke, P. 1997, Sol. Phys., 170, 75

Zirker, J.B. 1993, Sol. Phys., 148, 43